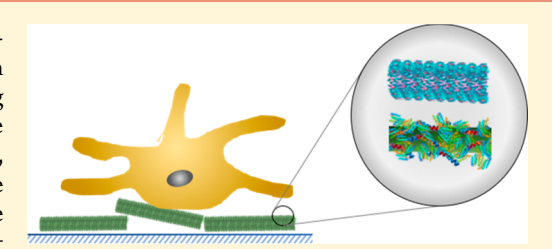
# Nanotopographical Cues Mediate Osteogenesis of Stem Cells on Virus Substrates through BMP-2 Intermediate

Kamolrat Metavarayuth, † Panita Maturavongsadit, ‡ Xiao Chen, § Pongkwan Sitasuwan, † Lin Lu, † Jiacan Su,\*,\* and Qian Wang\*,†

Supporting Information

ABSTRACT: Recent studies have demonstrated rapid osteogenic differentiation of bone marrow-derived mesenchymal stem cells (BMSCs) on substrates with plant virus modified nanotopographical cues as a promising strategy for bone repair; however, the mechanisms remain unclear. We hypothesized that the highly structurally ordered virus coat proteins, responsible for targeting specific cellular components, are critical for the osteogenesis promotion. In this study, hybrid viral gold nanorods were prepared to explore the effects of highly ordered arranged virus coat proteins on osteogenic differentiation of BMSCs. The results herein indicate



that it is the nanotopographical cues modified by structurally ordered virus nanoparticles, not the chemical properties of virus surface, that mediate osteogenesis. Bone morphogenetic protein 2 (BMP-2) expression is significantly increased and serves as a modulator that mediates the osteogenic differentiation in response to the viral particle coatings. After BMP-2 is inhibited by Noggin, the osteogenesis promoting effects are significantly compromised, demonstrated by lower alkaline phosphatase activity and calcium sequestration. This study reveals that plant virus modified nanotopographical substrates promote osteogenic differentiation of BMSCs through increasing BMP-2 autocrine. It provides key insights to engineering functional materials for rapid bone repair.

KEYWORDS: Nanoparticles, mesenchymal stem cells, osteogenesis, nanotopography, biomaterials

lant viruses are natural nanoparticles that have been used in chemistry and biomaterials applications. 1-5 As multifacet nanosized building blocks, plant viruses can be isolated in high purity with batch-to-batch consistencies at low cost. The chemical and genetical modifications of viral particles to incorporate new functional groups have been extensively studied. 1-3,6-8 Additionally, the symmetrical arrangement of the viral proteins confers superiority as scaffolds with identical copies of functional groups in electronics, catalysis, drug/gene delivery, imaging, and immunotherapy.<sup>2</sup>

As substrates for biomaterials, viruses with specifically arranged functional groups result in different cellular responses compared to unordered arrangement. Some animal viruses with pentameric motif integrin binding sites could promote cell internalization. 9,10 The adhesion force associated with the clusters of integrin binding motifs can be seven-fold stronger than that with nonclustered ligand-receptor interactions. 11,12 In cell signaling, Arg-Gly-Asp (RGD) peptide targeted integrin receptors form dynamic clusters that are essential in cell adhesion, migration, and mechanotransduction, which ultimately affects stem cell differentiation. 13,14

Previous studies from our group revealed that substrates coated with plant viruses promoted mesenchymal stem cell growth and accelerated osteogenic differentiation. 15-20 Bonederived mesenchymal stem cells (BMSCs) cultured on various virus-coated substrates such as wild type, phosphate modified, and genetically modified tobacco mosaic virus (TMV), turnip yellow mosaic virus (TYMV), turnip vein clearing virus (TVCV), and potato virus X (PVX) showed increased alkaline phosphatase activity, calcium mineralization, and higher expression levels of genes related to osteogenesis. More importantly, these studies have reported a rapid up-regulation of bone morphogenetic protein 2 (BMP-2), a clinically approved therapeutic supplement for bone repair, prior to osteogenesis of the stem cells on these virus coated substrates.

Living organisms are sophisticated systems comprised of cells of multiple types embedded in a complex, well-defined extracellular matrix (ECM). The ECM possesses topographical and adhesive features ranging from nanometers to micro-

Received: May 15, 2019 Revised: July 9, 2019 Published: July 11, 2019



Department of Chemistry and Biochemistry, University of South Carolina, 631 Sumter Street, Columbia, South Carolina 29208,

<sup>&</sup>lt;sup>‡</sup>Joint Department of Biomedical Engineering, University of North Carolina at Chapel Hill and North Carolina State University, Chapel Hill, North Carolina 27599, United States

<sup>§</sup>Department of Orthopedics Trauma, Changhai Hospital, Second Military Medical University, Shanghai 200433, China

meters. Many ECM proteins form large-scale structures up to several hundred micrometers in size and interact with multiple individual cells. However, recent findings emphasize that mammalian cells can respond to nanoscale structures on synthetic surfaces. The argument for this finding lies in the premise that cells contain nanoscale features compatible with nanoscale ECM structures. With these nanoscale features, cells can sense nanotopography of the underlying surfaces. Taking advantage of this phenomenon, scientists have fabricated biomaterials with unique topographies to control cell behaviors.

Mesenchymal stem cells are multipotent stromal cells that can differentiate into a variety of cell types, including osteoblasts, chondrocytes, myocytes, adipocytes. <sup>22</sup> As the most widely studied, BMSCs mainly differentiate into osteoblasts and adipocytes in the skeleton. In various pathological scenarios such as osteoporosis and rheumatoid arthritis, BMSCs osteogenic differentiation is inhibited and adipogenesis is increased. <sup>23</sup> Thus, regulating the BMSCs differentiation and increasing the rate of osteogenesis are potential treatment options to correct the imbalance. <sup>24,25</sup>

In this study, we modified the nanotopographical ECM with nanoscale materials to investigate osteo-chondrogenesis of BMSCs and explored the underlying mechanisms (Figure 1a). The information provides fundamental knowledge that can be

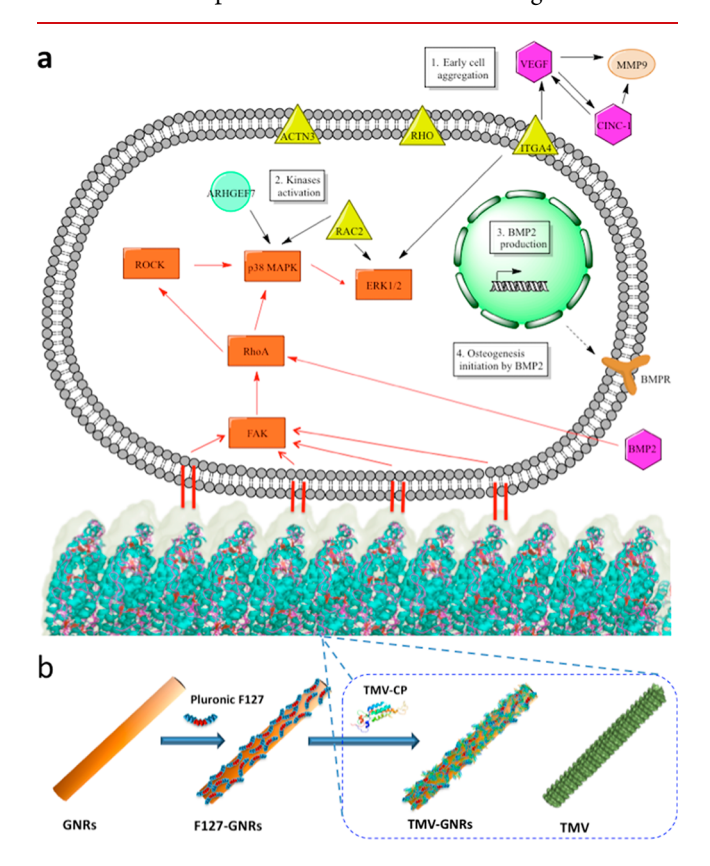


Figure 1. Nanotopographical cues mediate osteogenic differentiation of stem cells. Proposed pathway involves BMP-2 intermediates osteogenesis in which initiated by unique nanoscale topography of virus substrate (a). Cartoon illustrating three types of nanoparticles used in this study including TMV coat proteins (TMV-CP), TMV coat protein-coated gold nanorod (TMV-GNRs) prepared from Pluronic F127-coated GNRs (F127-GNRs), and wild type tobacco mosaic virus (TMV) (b).

further optimized for regulating BMSCs differentiation fate and applied to be used in clinical bone repair in the future.

Results and Discussion. Previous studies showed that unique nanotopographical arrangement through orderly deployed virus proteins could increase BMSCs osteogenic differentiation. 16,20,26 We hypothesized that BMSCs osteogenesis on plant virus-coated substrates resulted from highly ordered arrangement of virus-coated proteins. Therefore, we designed a systemic analysis to study two possible parameters for the cellular response. First, we examined the chemistry of TMV coat protein (TMV-CP). Because virus-coated proteins displayed numerous functional groups on their outer surface, the chemical features of the proteins could account for different cellular responses. Poly D-lysine (PDL) was selected to coat on the bottom of tissue culture plate to provide positive charge surface that would retain negative charge nanoparticles onto the substrate surface. Then we coated individual TMV-CP isolated by an acetic acid catalyzed disassemble of the TMV particle on the PDL substrate. The TMV-CP prepared by this method has shown to preserve its native structure similar to the TMV-CP prepared by the virus particle disassembled in alkaline solution. Furthermore, these TMV-CPs could be reassembled back to the virus-inherent helix structure upon being reconstituted with its generic material. 27-29 This phenomenon supports that the acetic acid RNA removal method can be used to prepare TMV-CP without causing the denaturation of the protein. In addition, the CD spectra of TMV and TMV-CP prepared by this method were consistent with reported spectra (Figure S1). 30,31 Second, we explored the specific arrangement of TMV-CP in wild type virus nanoparticle. The highly ordered coat protein arrangement of many viruses was demonstrated to be responsible for different cellular responses. 32,33 To study the effects of virus protein arrangement, hybrid viral gold nanorods (TMV-GNRs) were prepared from cetrimonium bromide (CTAB)capped gold nanorods (CTAB-GNRs) that have similar dimension to wild type TMV. The CTAB-GNRs were synthesized by the protocol developed by Murphy et al.34 Then we randomly coated the gold nanorods with TMV-CP, which was completed with Pluronic F127 triblockcopolymer as a linker that possessed affinity to both CTAB-GNRs and TMV-CP. 35,36 Hydrophobic cores of the polymers interacted with long alkyl chain of CTAB while hydrophilic sides of Pluronic F127 were believed to form H-bond with TMV-CP. Wild type TMV substrate was used as a positive control (Figure 1b).

The assembled structures (TMV-GNRs) were verified with transmission electron microscope (TEM) and the zeta potential was measured by dynamic light scattering (DLS) as shown in Figure 2. After TMV-CP had been assembled on the polymer-coated GNRs, representative TEM images clearly demonstrated rougher surface with darker and thicker stained rod particles. Changes of the nanoparticle surface charge of assembled hybrid viral gold nanoparticles were detected by DLS. CTAB-GNRs showed positively charged surface from quaternary amine of the surfactant. The positive charge was reduced once CTAB was covered with neutral triblockcopolymer Pluronic F127. After TMV-CP was coated on the outermost layer of the nanoparticle, surface charge became negative as did TMV-CP. The zeta potential of native TMV was -21.9 mV, consistent with the literature report,<sup>37</sup> while the zeta potential of TMV-GNRs was -29.8 mV, very similar to native TMV particles. All nanoparticles displayed negatively

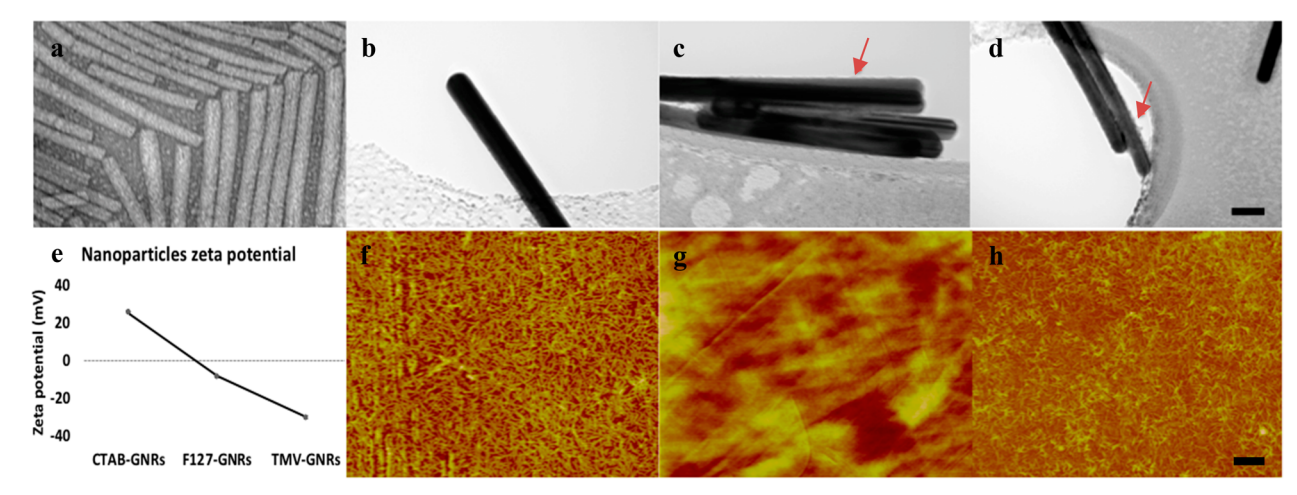


Figure 2. Nanoparticle-coated substrates for stem cell cultures. (a–d) TEM images of TMV (a); CTAB capped gold nanorods (CTAB-GNRs) (b); coated structure resulting from mixing 10 mg/mL Pluronic F127 with CTAB-GNRs (c) and the arrow points at triblockcopolymer light stained on the nanorod surface; TMV coat protein-coated gold nanorods (TMV-GNRs) (d) and the arrow designates TMV coat protein appearance on the nanorod structure. Scale bar is 50 nm. (e) Change of zeta potential during TMV-GNRs assembling process obtained from DLS. CTAB-GNRs had positively charged surface from quaternary amine of CTAB. The positive charge was reduced once CTAB was covered with neutral triblockcopolymer Pluronic F127. After TMV-CP was coated on the outermost layer of the nanoparticle, the surface charge became negative as did TMV-CP. (f–h) AFM height image of TMV (f), TMV-CP (g), and TMV-GNRs (h); notice that the nanoparticles were mostly intact and laid flat on the surface. Scale bar is 1  $\mu$ m.

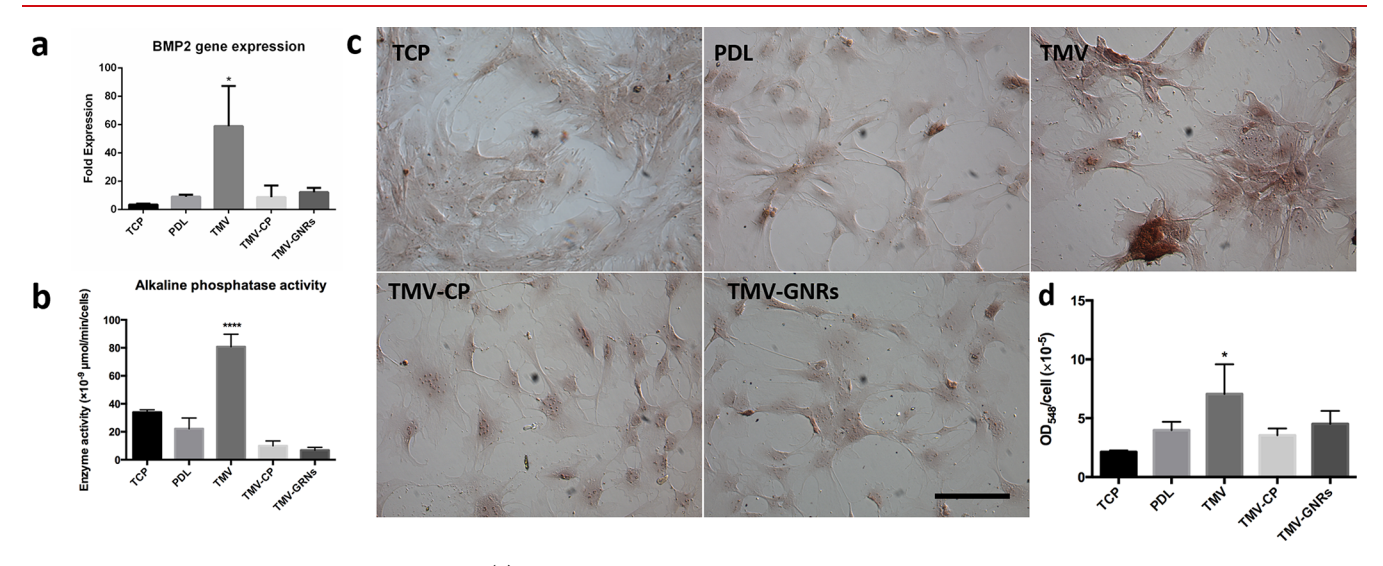


Figure 3. Osteogenesis of BMSCs demonstrated (a) at 6 h after osteoinduction wherer only the cells on TMV substrate showed BMP-2 gene upregulation. (b) Similarly, at day 7 after osteoinduction cells on TMV substrate showed significantly higher alkaline phosphatase activity compared to TCP and PDL control. (c) The cells on TMV substrates were stained positive for calcium deposition by Alizarin S Red staining and had (d) greater calcium mineralization quantified from solubilized dye by 0.1 N NaOH solution. Scale bar is 200  $\mu$ m. The data were expressed as mean  $\pm$  s.d. (n = 3, \*  $p \le 0.05$ , \*\*\*\*  $p \le 0.0001$  based on ANOVA with Tukey's multiple comparisons test)

charged surface at neutral pH. Therefore, these particles can be held stably on PDL-coated substrate via electrostatic interaction as shown by atomic force microscopy (AFM). AFM images revealed that coating of the three nanoparticles on PDL substrates achieved almost full coverage and nanoparticles were mostly intact and lay flat on the surface after incubation with cell culture media for 24 h. Because the roughness of a substrate is one of the major factors that can influence cell responses, the average roughness of each nanoparticle-coated substrate was analyzed. The results showed slight differences between each sample with TMV-GNRs having the highest average roughness at 10.8 nm followed by CTAB-GNRs at 7.4 nm and TMV at 5.8 nm. TMV-CP coated substrate had the lowest average roughness at

3.3 nm. (Figure S2) In addition, this result confirms the successful assembly of TMV-CP on GNRs particle as seen by the increased roughness in TMV-GNRs compared to the bare CTAB-GNRs.

BMSCs were cultured on these substrates in serum containing Dulbecco's Modified Eagle's Medium (DMEM) media for 24 h then osteoinduction factors (dexamethasone, ascorbic acid, and  $\beta$ -glycerophosphate) were supplemented to induce osteogenic differentiation. To characterize cells cultured on various substrates, we probed for key osteogenic markers (BMP-2, alkaline phosphatase activity, and calcium sequestration). Six hours after osteoinduction BMP-2 mRNA level was dramatically up-regulated only in cells on TMV substrate (Figure 3a). Furthermore, 7 days afterward these cells

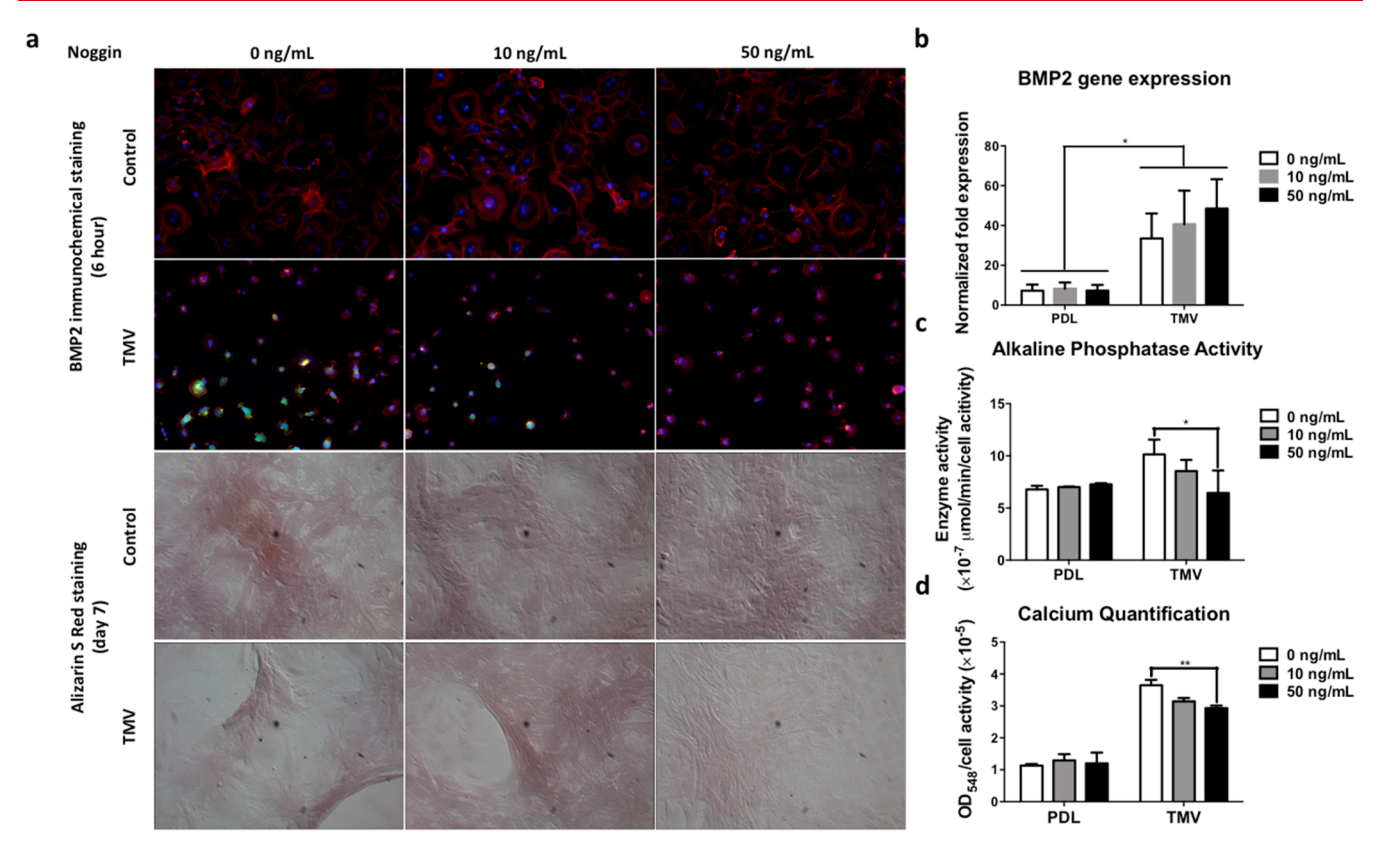


Figure 4. BMP-2 inhibitor (Noggin) inhibits TMV induced osteogenesis of BMSCs. (a) Immunofluorescence images of cells on PDL and TMV substrates incubated with Noggin at different concentrations for 6 h (top panel). Color representation: nucleus (blue), actin (red), and BMP-2 (green). Cells on TMV substrate have higher BMP-2 expression compared to cells on PDL substrates and BMP-2 protein level decreases at higher Noggin concentration. The bottom panel shows calcium staining of each sample at day 7. Treatment of Noggin reduces calcium mineralization in cells cultured on TMV substrates. (b) The mRNA expression of BMP-2 in cells on PDL and TMV substrates treated with Noggin at different concentration for 6 h. Cells slightly increase BMP-2 gene expression when incubated with Noggin. This might be due to the negative feedback from the reduction of free BMP-2 protein availability for BMP-2 receptor. (c) Alkaline phosphatase activity of cells treated with Noggin when cultured on PDL and TMV substrates 7 days after osteoinduction. The enzyme activity reduces as Noggin concentration is increased. (d) Calcium mineralization is also reduced with increased Noggin concentrations. The data were expressed as mean  $\pm$  s.d. (n = 3, \*  $p \le 0.05$ , \*\*  $p \le 0.01$  based on ANOVA with Tukey's multiple comparisons test).

aggregated and formed calcified nodules which were positively stained by Alizarin S Red, a typical cytochemical stain for calcium in cells undergoing osteogenesis (Figure 3c,d). We also found at least two-fold higher activity of alkaline phosphatase enzyme in BMSCs on TMV substrates compared to cells on other substrates (Figure 3b). These results highlighted that nanotopographical cues by the highly ordered arrangement of virus-coated proteins had dominant effects on BMSCs osteogenic differentiation rather than surface chemistry of the virus-coated proteins. It is possible that Pluronic F-127 which may expose on TMV-GNRs have influence on the cell responses. For this matter, an additional osteogenic study including Pluronic F-127 coated on TMV-coated substrate as a control group was performed. The result showed no reduction in alkaline phosphatase activity nor calcium quantity in cells cultured on F-127 coated samples compared to TMV samples alone (Figures S3 and S4). This means that Pluronic-F127 alone does not inhibit or reduce the effect of TMV on osteogenesis enhancement as seen in cells cultured on TMV-GNRs samples. Because it is extremely difficult to control the arrangement and density of CP on the surface of GNRs. It is possible that the upregulation of the osteogenesis could be attributed to a combination of several factors including the orientation of individual TMV-CPs, the three-dimensional

(3D) arrangement of TMV-CPs, and the topography of the coated substrates. Although it is difficult to pinpoint which factor plays the most important role in the process, this study was the first attempt to address this important and complex issue. The CD results confirmed that the TMC-CPs maintains the natural conformation (Figure S1), therefore it is most likely that the nanoscale arrangement of TMV-CPs on the native TMV that makes the major contribution to the upregulated osteogenesis as observed in this study.

The up-regulation of BMP-2 gene expressions found in this study was consistent with all previous studies on virus substrates promoting early osteogenesis of BMSCs. These studies reported that virus substrate was a potent modulator of BMSCs differentiation with a rapid increase in BMP-2 gene expression within the first 24 h of osteoinduction. In addition, the results suggested that BMSCs osteogenic differentiation on virus substrates was mediated through the up-regulation of BMP-2 expression. To confirm BMP-2 involvement, Noggin, a BMP-2 inhibitor, was added into cell culture media to interfere with BMP-2 binding to its receptor. As expected, BMP-2 protein level was decreased when increasing concentration of Noggin was introduced to cells on TMV substrate. This was shown by immunohistochemical staining of BMP-2 (Figure 4a). Furthermore, the higher the

concentration of Noggin that was administered, the less the BMSCs on TMV substrate were differentiated. This was probed by decreased alkaline phosphatase activity and calcium mineralization of cells on TMV substrates. On the other hand, no change was observed in cells on PDL substrates (Figure 4c,d). Surprisingly, cells slightly increased BMP-2 gene expression when incubated with Noggin at different concentrations; however, the increasing levels are not significantly different. This might result from the negative feedback from the reduction of free available BMP-2 protein for BMP-2 receptors (Figure 4b).<sup>38</sup>

In addition to osteogenesis, it is widely known that BMP-2 plays an essential role in the regulation of chondrocyte proliferation and maturation. <sup>39,40</sup> A previous study by our group has observed the upregulation of BMP-2 which led to the enhanced chondrogenesis of BMSCs cultured in TMV incorporated hyaluronic acid hydrogel (TMV-HA).41 To better understand the phenomenon in 3D systems, in this study we further introduced GNRs synthesized by the method mentioned earlier to the hydrogel (GNR-HA) in order to investigate the effect of nanoscale topography of TMV-CP in 3D scaffold. The CTAB-GNRs showed no influence on BMSCs viability when incorporated in hyaluronic-based hydrogel (HA) (Figure 5a). The chondrogenesis performance of differentiated MSCs in the GNR-HA was evaluated by measuring mechanical property of the cell-encapsulated hydrogels. The complex modulus of the cell-encapsulated GNR-HA was measured after 28 days of chondrogenic cultures. No significantly promoted complex modulus was

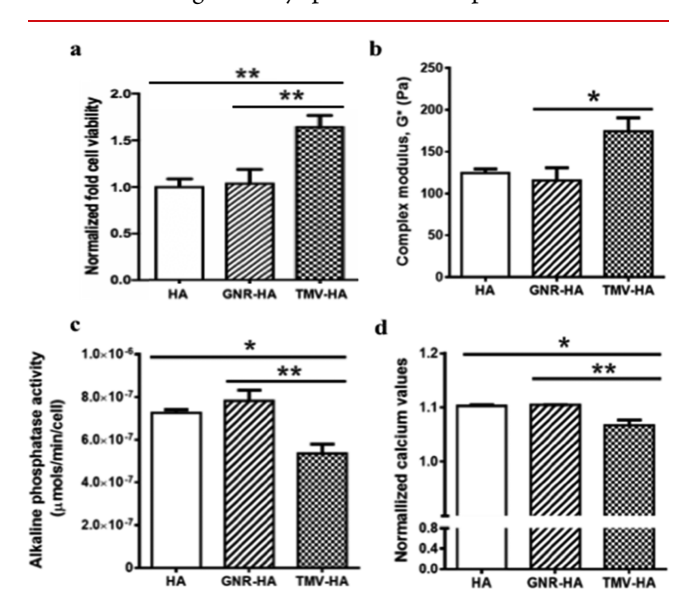


**Figure 5.** Chondrogenesis of encapsulated BMSCs in the hydrogels demonstrated (a) at day 28 after chondrogenic culture that the encapsulated cells in TMV-HA showed significantly higher metabolic activities. Each plot expressed mean  $\pm$  SEM, n=6. (b) At day 28 after chondrogenic culture, only the encapsulated cells in TMV-HA showed significantly improved biomechanical properties. Each plot expressed mean  $\pm$  SEM, n=3. (c) In contrast, at day 28 after chondrogenic culture encapsulated cells in TMV-HA showed significantly lower alkaline phosphatase activity compared to GNR-HA and HA control. (d) The encapsulated cells in TMV-HA showed significantly lower calcium mineralization compared to GNR-HA and HA control. Each plot expressed mean  $\pm$  SEM, n=3 with one repeated experiment, \*  $p \leq 0.05$ , \*\*  $p \leq 0.01$  based on ANOVA with Tukey's multiple comparisons test.

observed in the cell-encapsulated GNR-HA compared to that in the cell-encapsulated HA. In contrast, the average complex modulus of the cell-encapsulated TMV-HA was shown to be significantly higher than that in GNR-HA and HA (Figure 5b). The impact of incorporated GNRs in HA-based scaffolds on chondrogenic differentiation progression was also investigated. Because it is possible for the chondrogenic-differentiated MSCs to develop to the unwanted hypertrophy stage, 42-44 the alkaline phosphatase (ALP) activity and calcium deposition, unlike osteogenesis, are considered common hypertrophy markers for chondrogenesis. 45,46 These markers were quantified in the hydrogels after 28 days. The results of ALP activities demonstrated that the differentiated MSCs in GNR-HA and HA secreted ALP significantly higher than that in TMV-HA (Figure 5c). Although calcium deposition could not be accurately quantified due to the background color in all hydrogels (Figure 5d), calcium staining showed calcium deposits spreading throughout the matrix of GNR-HA and HA samples but no in TMV-HA (Figure 5d). On the basis of these results, we concluded that GNRs that incorporated HA hydrogels did not promote the MSC chondrogenesis in contrast to the TMV-incorporated HA hydrogels. These results further highlighted that nanotopographical cues by the highly ordered arrangement of virus-coated proteins had dominant effects on BMSCs chondrogenic differentiation in 3D systems rather than dimensions of the virus.

The pathways of substrate nanotopography induced BMP-2 which mediated osteo-chondrogenic differentiation requires further in-depth studies to track the clues of molecular mechanisms by which cells sense different topography. Early evidence of cells sensing substrate topography is the differences in focal adhesion (FA) structures. A key regulator of mechanotransduction is focal adhesion kinase (FAK) which triggers downstream signaling to the mitogen-activated protein kinase (MAPK) cascade via activation of RhoA/ROCK pathway. The participation of FAK/RhoA/ROCK/MAPK signaling pathway in substrate topography regulating cell differentiation can be assessed by blocking or knocking out key regulators in this complex system. Accelerating osteo-chondrogenesis with autologous mesenchymal stem cells is highly promising for future clinical applications.

**Materials and Methods.** Virus Purification from Infected Leaves. For the purification of TMV, first the infected leaves were blended with 3 volumes of 0.1 M potassium phosphate buffer pH of 7.0 and 0.1% β-mercaptoethanol. The mixture was filtered, and the filtrate was subjected to centrifugation to remove bulk plant material. The supernatant was collected and clarified by adding an equal volume of CHCl<sub>3</sub>/1-butanol (v/v = 1:1). The aqueous layer was then collected followed by precipitation of virus with 4% polyethylene glycol, MW 8 kDa (PEG) and 0.2 M sodium chloride. The pellet was centrifuged and resuspended in buffer before it was subjected to low speed centrifuge to remove PEG. The virus in the supernatant was finally pelleted by ultracentrifugation and resuspended in buffer.

*Preparation of TMV-CP.* TMV particles isolated from infected N. tabacum plants were used to obtain TMV-CP for the in vitro assembly of TMV-GNRs. Purification was carried out with the acetic acid method described by Fraenkel-Conrat.<sup>28</sup>

Preparation of TMV-GNRs. TMV-GNRs were prepared from CTAB-capped gold nanorods (CTAB-GNRs) that have similar dimensions to wild type TMV following protocols by

Table 1. Formulation of HA, Wide-Type TMV-Based HA, and GNR-Based HA Hydrogels

formulation	40-50% DM MeHA	TMV-wt	GNR	0.5 M DTT (molar ratio)	solvent, pH system
HA	5%			2Ene/1SH	PBS, pH 7.4
TMV-HA	5%	0.1%		2Ene/1SH	PBS, pH 7.4
GNR-HA	5%		0.1% <sup>a</sup>	2Ene/1SH	PBS, pH 7.4

<sup>a</sup>The amount of GNRs was calculated based on ICP-MS results.

Murphy et al.<sup>34</sup> First CTAB-capped gold nanoparticle seeds were first synthesized by reduction of 0.25 mM gold(III) chloride solution (HAuCl<sub>4</sub>) in 0.1 M CTAB solution with 0.6 mL 0.1 M ice-cold aqueous sodium borohydride (NaBH<sub>4</sub>). After aging for 5 h, the gold seeds were subjected to a three step protocol for nanorod synthesis. In each step, 1 mL of gold seed was added to 9 mL stock solution of 0.25 mM HAuCl<sub>4</sub> in 0.1 M CTAB solution containing 0.5 mM ascorbic acid. The longer gold nanoparticle obtained from each step then subsequently was used as the gold seeds for the next step growth. After 3 rounds of the procedure, gold nanorods with dimensions of approximately 18 × 300 nm are obtained. Next the gold nanorods were assembled with Pluronic F127 by first centrifuging the nanorods at 3300×g for 6 min and resuspending in nanopore water twice to remove excess CTAB. Then an equal volume of 20 mg  $\mathrm{mL}^{-1}$  Pluronic F127 in nanopore water was added to the gold nanorod solution. The mixture was incubated at room temperature for 2 h to obtain Pluronic F127-coated GNRs (F127-GNRs). The excess Pluronic F127 was removed by centrifugation of the mixture at 3300×g for 6 min and resuspended in 10 mM potassium phosphate buffer pH of 7.4. Next, TMV-CP in 10 mM potassium phosphate buffer of pH of 7.4 was slowly added to F127-GNRs that were stirred at 300 rpm. The mixture of TMV-CP and F127-GNRs was incubated for 2 h at room temperature then subjected to final centrifugation to remove excess TMV-CP.

Fabrication of Virus-Based Scaffolds. TMV (0.7 mL) in aqueous solution or TMV-CP in 100 mM tris-(hydroxymethyl)aminomethane hydrochloride (Tris-HCl) pH of 8.0 or TMV-GNRs in 10 mM potassium phosphate buffer pH of 7.4 were dropped into empty 12-well plates or 12-well plates that contain 18 mm circle-cleaned glass coverslips at the bottom of each well. The 12-well plates or the 18 mm circle-cleaned glass coverslips were first coated with PDL using the protocol suggested by Corning. The virus or nanoparticle solutions were incubated with the PDL-coated substrates under a sterile cell culture hood overnight. Then, the bottoms of each well were rinsed briefly with 18.2 m $\Omega$  water before being used for BMSCs culture.

Surface Characterization of Virus-Based Scaffolds by AFM. The surface morphology of virus-based scaffolds was observed by AFM (Nanoscope IIIA MultiMode AFM (Veeco)). After nanoparticles are coated, the glass coverslips were dried with a stream of nitrogen gas before being mounted onto the AFM sample holder for imaging in the tapping mode.

Formation of Rodlike Nanoparticle-HA Hydrogels. To form the rodlike nanoparticle-based HA hydrogels (TMV-HA and GNR-HA), GNRs synthesized as described previously were centrifuged at 6000 rpm and resuspended in phosphate buffered saline (PBS) several times to remove excess CTAB in solution. The surface of synthesized GNRs was then treated with dithiothreitol (DTT) thiol molecules for 30 min with stirring. The excess of DTT was removed and washed by centrifugation at 6000 rpm several times. The structural

integrity of TMV particles and GNRs were verified by TEM electron micrograph. To fabricate rodlike nanoparticle-based HA hydrogels, methacrylate HA polymers with 40–50% degree of modification (method is described in a previous study<sup>41</sup>) were dissolved in PBS at 5 wt % concentration, and TMV or GNRs in potassium phosphate buffer was added to make a final concentration of 0.1 or 0.2 wt % (the detailed formulations are in Table 1). A cross-linking agent, DTT, was then added at a molar ratio of thiol/ene = 1:2 (Table 1). For comparison purposes, the HA hydrogels were also prepared by the same procedure, except adding the rodlike nanoparticle solution.

BMSC Isolation and Expansion. Primary BMSCs were isolated from the bone marrow of young adult 80 g of male Wister rats (Harlan Sprague-Dawley Inc.). The procedures were performed in accordance with the guideline for animal experimentation by the Institutional Animal Care and Use committee, School of Medicine, University of South Carolina. Cells were maintained in primary media (DMEM (Hyclone, Thermo Scientific) supplemented with 10% fetal bovine serum (FBS, Atlanta biologicals), 1× penicillin-streptomycinamphotericin B (from MP Biomedicals, containing 100 U/ mL of penicillin, 1000 U/mL of streptomycin solution, 0.25  $\mu$ g/mL of amphotericin B), kept at 37 °C in a CO<sub>2</sub> incubator with 95% air/5% CO<sub>2</sub> and passaged no more than seven times after isolation. To induce osteogenesis, primary media were replaced with osteogenic media consisting of primary media supplemented with 10 mM sodium  $\beta$ -glycerophosphate (Sigma-Aldrich), 50  $\mu$ g mL<sup>-1</sup> L-ascorbic acid 2-phosphate (Sigma-Aldrich), and  $10^{-8}$  M dexamethasone (Enzo Life Sciences). Media were replenished every 3-4 days.

In Situ Cell Encapsulation and Culture in Hydrogel. The hydrogels were prepared as previously described except that the preparation occurred under sterile condition and prewarmed complete DMEM media was used to dissolve the polymer. TMV and CTAB-GNRs were filtered to remove any pathogens before mixing. All other components including 5 M sodium hydroxide (NaOH) and 0.5 M DTT in PBS were also filtered with 0.2 µm PES membranes. BMSCs' passage 3 or 4 was harvested from the tissue culture plate after reaching 80% confluency. The cells were then mixed with the mixture of prewarmed hydrogel in DMEM media at concentration of 10<sup>6</sup> cells/mL right after addition of DTT. The cells-hydrogel mixture (150  $\mu$ L) was then pipetted into each Transwell (Corning) that was inserted and anchored in a 24-well tissue culture plate and incubated at 37 °C in a CO2 incubator with 5% CO<sub>2</sub>/95% air. After 6 h of initial incubation, chondrogenic media (800  $\mu$ L) was added into each well. The media was exchanged every 2 days for the entire experimental period.

Chondrogenic Supplemented Media. Chondrogenic supplemented media is comprised of DMEM, 1% FBS, 1× penicillin–streptomycin–amphotericin B, 100 nM dexamethasone, 10 ng/mL of TGF  $\beta$ 1 (R&D System), 50  $\mu$ g/mL of ascorbic acid, 1 mM sodium pyruvate (Hyclone, Thermo Scientific), 1× ITS<sup>+3</sup> (from Sigma-Aldrich, contains 1.0 mg/

mL of insulin from bovine pancreas, 0.55 mg/mL of human transferrin (substantially iron-free), 0.5  $\mu$ g/mL of sodium selenite, 470  $\mu$ g/mL of linoleic acid, 470  $\mu$ g/mL of oleic acid, and 50 mg/mL of bovine serum albumin, BSA), 2 mM L-glutamine (Hyclone, Thermo scientific), and 40  $\mu$ g/mL of L-proline (Sigma-Aldrich).

Biomechanical Property Analysis of Hydrogel. The hydrogels were collected at days 0, 14, and 28 of chondrogenic culturing and subjected to test storage (G') and loss (G'')moduli using DHR-3 rheometer (TA Instruments) with 12 mm diameter parallel-plate geometry and temperaturecontrolled Peltier plate. The samples were cut into uniform cylinders and placed on a metal plate, where the tests were performed. Amplitude sweeps at constant frequency (1 rad/s) were performed to determine the linear viscoelastic range of deformation for each sample after which frequency sweeps (0.1-10 rad/s) were performed at a strain amplitude within the linear range (2%). In amplitude and frequency sweeps measurement, the geometry gaps were conditioned by axial force at 0.5 N for every run. The linear equilibrium modulus plateau  $(G_e)$  of hydrogels was calculated from the average of storage modulus (G') over the frequency range.

Quantitative Real-Time RT-PCR Analysis (RT-qPCR). PDL and virus-coated substrates were seeded with  $4.0 \times 10^4$  cells per well in primary media and allowed to attach overnight. The unseeded cells were used as a control to normalize the change in gene expression. The media were replaced to osteogenic media with or without Noggin at different concentration and cultured for 6 h. The cell cultures were terminated after 6 h and total RNA was subsequently extracted using E.Z.N.A. RNA Isolation Kit, OMEGA. At least two separate experiments were conducted with each type of sample. The purity and quantity of the extracted RNA were analyzed using Thermo Scientific Nanodrop 2000c spectrophotometer and was reverse transcripted by qScript cDNA Supermix (Quanta Biosciences). RT-qPCR (iQ5 real-time PCR detection system Bio-Rad Laboratories) was done by the method described as 60 cycles of PCR (95 °C for 20 s, 58 °C for 15 s, and 72 °C for 15 s), after initial denaturation step of 5 min at 95 °C by using 12.5  $\mu$ L of iQ5 SYBR Green I Supermix, 2 pmol  $\mu$ L<sup>-1</sup> of each forward and reverse primers and 0.5  $\mu$ L of cDNA templates in a final reaction volume of 25  $\mu$ L. Glyceraldehyde 3-phosphate dehydrogenase (GAPDH) was used as the housekeeping gene. Data collection was enabled at 72  $^{\circ}$ C in each cycle and  $C_{\rm T}$ (threshold cycle) values were calculated using the iQ5 optical system software version 2.1. The expression levels of differentiated genes and undifferentiated genes were calculated using Pfaffl's method (M. W. Pfaffl, G. W. Horgan, and L. Dempfle, Relative expression software tool) for group-wise comparison and statistical analysis of relative expression results in real-time PCR, using GAPDH as the reference gene. Quantification of gene expression was based on the  $C_T$  value of each sample that was calculated as the average of at least two replicate measurements for each sample analyzed. "Pair Wise Fixed Reallocation Randomization Test" was performed on each sample and a value of p < 0.05 was regarded as significant. The primers used for RT-qPCR are BMP2, 5'-ACCAACC-ATGGGTTTGTGGTGGAAGT-3', 5'-TCCGCT-GTTTGTGTTTGGCT TGACG-3', GAPDH, 5'-ACTAAAGGGCATCCTGGGCTACACTGA-3', and 5'-TGGGTGGTCCAGGGTTTCTTACTCCTT-3'.

Alkaline Phosphatase (ALP) Activity. (a) In 2D substrates, after 7 days of induction in the osteogenic media with or

without Noggin at different concentrations, the BMSCs seeded on PDL and virus-coated substrates were determined by number of cells on each substrate by CellTiter Blue assay. Then the cells were fixed with 4% paraformaldehyde (PFA) for 15 min at room temperature prior to analyzing the ALP activity by incubating the briefly fixed cells with 1-Step pnitrophenylphosphate solution (pNPP, Thermo Scientific) for 15 min at room temperature. The solution was transferred to a new microfuge tube that contained 250 µL of 2 N NaOH and the absorbance at 405 nm was measured. The measure ALP activity from each sample was normalized to the corresponding cell number. (b) In 3D hydrogel, after 28 days of induction in the osteogenic media, the hydrogels with cells were prewashed with PBS and then incubated with pNPP solution at room temperature for 1 h. Absorbance was read using a M2 SpectraMax plate reader at 405 nm, indicating ALP activity levels.

Alizarin Red Staining and Quantification. Calcium deposition on each substrate was visualized and quantified to confirm and compare osteogenic differentiation by Alizarin red staining. A fixed cell on day 7 was stained with 0.1% Alizarin red solution (Sigma-Aldrich) with pH of 4.1–4.5 for 30 min in the dark. The samples were washed with water (18.2 M $\Omega$ ) prior to imaging. To quantify the amount of dye on each substrate, 300  $\mu$ L of 0.1 N NaOH was added to each sample to extract the dye from the sample. The extracted dye solution was measured with the absorbance at a 548 nm wavelength. The measure absorbance from each sample was normalized to the corresponding cell number from CellTiter Blue assay.

Immunofluorescence Assays and Image Analysis. For immunofluorescence assays and image analysis, PDL or nanoparticle-coated glass coverslips were used as substrates for BMSCs culture. The substrates were seeded with  $4.0 \times 10^5$ cells per sample. The cultures were terminated at 6 h after osteoinduction. After termination, cells were fixed in 4% PFA at room temperature for 30 min. Each of the samples was then permeabilized for 20 min by 0.1% Triton-X 100 for 15 min and blocked in 1.5% BSA (Sigma-Aldrich) in PBS for 1 h at room temperature. After the blocking, the cells were incubated overnight with mouse monoclonal antibody targeting BMP-2 (R&D Systems) at 1:100 dilution in blocking buffer. After overnight incubation, secondary goat antimouse antibody conjugated with fluorescein (Chemicon) was used at 1:400 dilution for 2 h at room. Rhodamine phalloidin (1:100 in PBS) was used to stain filamentous actin. Nuclei were stained with DAPI (4,6-diamidino-2-phenylindole, 100 ng mL<sup>-1</sup>). Images of the stained substrates were taken on an Olympus IX81 fluorescent microscope. SlideBook 5 was used to analyze immunofluorescence images.

**Conclusion.** In conclusion, we observed accelerated osteogenic differentiation on TMV-coated substrate but not on TMV-CP or TMV-GNRs substrates. This suggested that nanotopography modified by highly ordered arrangement of TMV-CP on the natural virus particles accounted for the rapid osteogenic differentiation. During the study of nanotopographical cues of virus substrates on osteogenesis of BMSCs, we successfully prepared hybrid viral gold nanorods (TMV-GNRs) by Pluronic F127 assisted assembly of TMV-CP and CTAB-GNRs which provided similar dimensions to TMV. In addition, the accelerated osteogenesis by virus substrates was mediated through the upregulation of BMP-2 gene expression in an autocrine manner, which was inhibited by a BMP-2 inhibitor, Noggin. Similar to osteogenesis, we observed

accelerated chondrogenic differentiation in TMV-incorporated HA hydrogels but not in GNR-HA or HA hydrogels. This further confirms that the influences of nanotopography provided by TMV play critical roles in directing BMSCs differentiation.

The insightful mechanisms of controlling the enigmatic stem cell behaviors involving pathways by topographical cues will further broaden the understanding and development of biomaterials for bone tissue engineering and clinical applications.

# **■** ASSOCIATED CONTENT

# Supporting Information

The Supporting Information is available free of charge on the ACS Publications website at DOI: 10.1021/acs.nanolett.9b02001.

CD spectra of wild type TMV (wt-TMV) and TMV coat protein (TMV-CP), Average roughness of TMV, TMV-CP, CTAB-GNRs, and TMV-GNR coated substrates, alkaline phosphatase activity of BMSCs cultured on PDL control, TMV-coated substrates and Pluronic F127 coated on TMV substrates, calcium mineralization quantification of BMSCs cultured on PDL control, TMV-coated substrates and Pluronic F127 coated on TMV substrates (PDF)

### AUTHOR INFORMATION

## **Corresponding Authors**

\*E-mail: drsujiacan@163.com. Tel: 803-777-8436. Fax: 803-777- 9521.

\*E-mail: wang263@mailbox.sc.edu.

#### ORCID ®

Qian Wang: 0000-0002-2149-384X

#### **Author Contributions**

The manuscript was written through contributions of all authors. All authors have given approval to the final version of the manuscript.

#### Notes

The authors declare no competing financial interest.

# **■** ACKNOWLEDGMENTS

This work was supported in part by the NSF and SC EPSCoR/IDeA Program under NSF Award #OIA-1655740. This work was supported in part by the National Natural Science Foundation (NNSF) Key Research Program in Aging (91749204), National Key R&D Program of China (Grant 2018YFC2001500), and Municipal Human Resources Development Program for Outstanding Leaders in Medical Disciplines in Shanghai (2017BR011). The views, perspective, and content do not necessarily represent the official views of the SC EPSCoR/IDeA Program nor those of the NSF.

# **■** REFERENCES

- (1) Ku, S. H.; Lee, S. H.; Park, C. B. Synergic effects of nanofiber alignment and electroactivity on myoblast differentiation. *Biomaterials* **2012**, 33 (26), 6098–104.
- (2) Pokorski, J. K.; Steinmetz, N. F. The art of engineering viral nanoparticles. *Mol. Pharmaceutics* **2011**, 8 (1), 29–43.
- (3) Chung, W.-J.; Merzlyak, A.; Lee, S.-W. Fabrication of engineered M13 bacteriophages into liquid crystalline films and fibers for directional growth and encapsulation of fibroblasts. *Soft Matter* **2010**, 6 (18), 4454–4459.

(4) Wang, J.; Wang, L.; Li, X.; Mao, C. Virus activated artificial ECM induces the osteoblastic differentiation of mesenchymal stem cells without osteogenic supplements. *Sci. Rep.* **2013**, *3*, 1242.

- (5) Merzlyak, A.; Indrakanti, S.; Lee, S. W. Genetically engineered nanofiber-like viruses for tissue regenerating materials. *Nano Lett.* **2009**, 9 (2), 846–52.
- (6) Zhu, H.; Cao, B.; Zhen, Z.; Laxmi, A. A.; Li, D.; Liu, S.; Mao, C. Controlled growth and differentiation of MSCs on grooved films assembled from monodisperse biological nanofibers with genetically tunable surface chemistries. *Biomaterials* **2011**, *32* (21), 4744–52.
- (7) Wang, Q.; Lin, T.; Tang, L.; Johnson, J. E.; Finn, M. G. Icosahedral Virus Particles as Addressable Nanoscale Building Blocks. *Angew. Chem., Int. Ed.* **2002**, 41 (3), 459–462.
- (8) Destito, G.; Schneemann, A.; Manchester, M., Biomedical Nanotechnology Using Virus-Based Nanoparticles. In *Viruses and Nanotechnology*; Manchester, M., Steinmetz, N., Eds.; Springer: Berlin Heidelberg, 2009; Vol. 327, pp 95–122.
- (9) Nemerow, G. R.; Pache, L.; Reddy, V.; Stewart, P. L. Insights into adenovirus host cell interactions from structural studies. *Virology* **2009**, 384 (2), 380–8.
- (10) Dicara, D.; Burman, A.; Clark, S.; Berryman, S.; Howard, M. J.; Hart, I. R.; Marshall, J. F.; Jackson, T. Foot-and-mouth disease virus forms a highly stable, EDTA-resistant complex with its principal receptor, integrin alphavbeta6: implications for infectiousness. *J. Virol* **2008**, 82 (3), 1537–46.
- (11) Kiessling, L. L.; Gestwicki, J. E.; Strong, L. E. Synthetic multivalent ligands as probes of signal transduction. *Angew. Chem., Int. Ed.* **2006**, *45* (15), 2348–68.
- (12) Petrie, T. A.; Raynor, J. E.; Dumbauld, D. W.; Lee, T. T.; Jagtap, S.; Templeman, K. L.; Collard, D. M.; Garcia, A. J. Multivalent integrin-specific ligands enhance tissue healing and biomaterial integration. *Sci. Transl. Med.* **2010**, 2 (45), 45ra60.
- (13) Hynes, R. O. The extracellular matrix: not just pretty fibrils. *Science* **2009**, 326 (5957), 1216–9.
- (14) Danen, E. H.; Yamada, K. M. Fibronectin, integrins, and growth control. *J. Cell. Physiol.* **2001**, *189* (1), 1–13.
- (15) Kaur, G.; Valarmathi, M. T.; Potts, J. D.; Wang, Q. The promotion of osteoblastic differentiation of rat bone marrow stromal cells by a polyvalent plant mosaic virus. *Biomaterials* **2008**, 29 (30), 4074–81.
- (16) Kaur, G.; Valarmathi, M. T.; Potts, J. D.; Jabbari, E.; Sabo-Attwood, T.; Wang, Q. Regulation of osteogenic differentiation of rat bone marrow stromal cells on 2D nanorod substrates. *Biomaterials* **2010**, *31* (7), 1732–41.
- (17) Kaur, G.; Wang, C.; Sun, J.; Wang, Q. The synergistic effects of multivalent ligand display and nanotopography on osteogenic differentiation of rat bone marrow stem cells. *Biomaterials* **2010**, *31* (22), 5813–24.
- (18) Sitasuwan, P.; Andrew Lee, L.; Bo, P.; Davis, E. N.; Lin, Y.; Wang, Q. A plant virus substrate induces early upregulation of BMP2 for rapid bone formation. *Integr Biol.* (*Camb*) **2012**, *4* (6), 651–60.
- (19) Sitasuwan, P.; Lee, L. A.; Li, K.; Nguyen, H. G.; Wang, Q. RGD-conjugated rod-like viral nanoparticles on 2D scaffold improve bone differentiation of mesenchymal stem cells. *Front. Chem.* **2014**, *2*, 31.
- (20) Metavarayuth, K.; Sitasuwan, P.; Luckanagul, J. A.; Feng, S.; Wang, Q. Virus Nanoparticles Mediated Osteogenic Differentiation of Bone Derived Mesenchymal Stem Cells. *Advanced Science* **2015**, 2 (10), 1500026.
- (21) Yim, E. K.; Leong, K. W. Significance of synthetic nanostructures in dictating cellular response. *Nanomedicine* **2005**, *1* (1), 10–21.
- (22) Beyer Nardi, N.; da Silva Meirelles, L. Mesenchymal stem cells: isolation, in vitro expansion and characterization. *Handb. Exp. Pharmacol.* **2006**, 174, 249–82.
- (23) Kim, M.; Lee, Y. J.; Jee, S. C.; Choi, I.; Sung, J. S. Antiadipogenic effects of sesamol on human mesenchymal stem cells. *Biochem. Biophys. Res. Commun.* **2016**, 469 (1), 49–54.

(24) Byun, M. R.; Hwang, J. H.; Kim, A. R.; Kim, K. M.; Hwang, E. S.; Yaffe, M. B.; Hong, J. H. Canonical Wnt signalling activates TAZ through PP1A during osteogenic differentiation. *Cell Death Differ.* **2014**, 21 (6), 854–63.

- (25) Bennett, C. N.; Ouyang, H.; Ma, Y. L.; Zeng, Q.; Gerin, I.; Sousa, K. M.; Lane, T. F.; Krishnan, V.; Hankenson, K. D.; MacDougald, O. A. Wnt10b increases postnatal bone formation by enhancing osteoblast differentiation. *J. Bone Miner. Res.* **2007**, 22 (12), 1924—32.
- (26) Sitasuwan, P.; Lee, L. A.; Bo, P.; Davis, E. N.; Lin, Y.; Wang, Q. A plant virus substrate induces early upregulation of BMP2 for rapid bone formation. *Integrative biology: quantitative biosciences from nano to macro* **2012**, *4* (6), 651.
- (27) Fraenkel-Conrat, H. Degradation of tobacco mosaic virus with acetic acid. *Virology* **1957**, *4* (1), 1–4.
- (28) Fraenkel-Conrat, H.; Williams, R. C. Reconstitution of Active Tobacco Mosaic Virus from Its Inactive Protein and Nucleic Acid Components. *Proc. Natl. Acad. Sci. U. S. A.* **1955**, *41* (10), 690–8.
- (29) McCarthy, D. Separation of the stable aggregates of tobacco mosaic virus protein by electrophoresis on polyacrylamide gels. *J. Gen. Virol.* **1968**, 3 (3), 417–25.
- (30) Makarov, V. V.; Skurat, E. V.; Semenyuk, P. I.; Abashkin, D. A.; Kalinina, N. O.; Arutyunyan, A. M.; Solovyev, A. G.; Dobrov, E. N. Structural lability of Barley stripe mosaic virus virions. *PLoS One* **2013**, *8* (4), No. e60942.
- (31) Arutyunyan, A. M.; Rafikova, E. R.; Drachev, V. A.; Dobrov, E. N. Appearance of "beta-like" circular dichroism spectra on protein aggregation that is not accompanied by transition to beta-structure. *Biochemistry (Moscow)* **2001**, *66* (12), 1378–80.
- (32) Lees, W. J.; Spaltenstein, A.; Kingery-Wood, J. E.; Whitesides, G. M. Polyacrylamides bearing pendant alpha-sialoside groups strongly inhibit agglutination of erythrocytes by influenza A virus: multivalency and steric stabilization of particulate biological systems. *J. Med. Chem.* **1994**, *37* (20), 3419–33.
- (33) Mammen, M.; Dahmann, G.; Whitesides, G. M. Effective inhibitors of hemagglutination by influenza virus synthesized from polymers having active ester groups. Insight into mechanism of inhibition. *J. Med. Chem.* 1995, 38 (21), 4179–90.
- (34) Busbee, B. D.; Obare, S. O.; Murphy, C. J. An Improved Synthesis of High-Aspect-Ratio Gold Nanorods. *Adv. Mater.* **2003**, *15* (5), 414–416.
- (35) Goh, D.; Gong, T.; Dinish, U. S.; Maiti, K. K.; Fu, C. Y.; Yong, K.-T.; Olivo, M. Pluronic Triblock Copolymer Encapsulated Gold Nanorods as Biocompatible Localized Plasmon Resonance-Enhanced Scattering Probes for Dark-Field Imaging of Cancer Cells. *Plasmonics* **2012**, *7* (4), 595–601.
- (36) Liu, Z.; Gu, J.; Wu, M.; Jiang, S.; Wu, D.; Wang, Q.; Niu, Z.; Huang, Y. Nonionic block copolymers assemble on the surface of protein bionanoparticle. *Langmuir* **2012**, *28* (33), 11957–61.
- (37) Gao, S.; Liu, X.; Wang, Z.; Jiang, S.; Wu, M.; Tian, Y.; Niu, Z. Fluorous interaction induced self-assembly of tobacco mosaic virus coat protein for cisplatin delivery. *Nanoscale* **2018**, *10* (25), 11732–11736.
- (38) Lee, S. H.; Fu, K. K.; Hui, J. N.; Richman, J. M. Noggin and retinoic acid transform the identity of avian facial prominences. *Nature* **2001**, 414 (6866), 909–12.
- (39) Zhou, N.; Li, Q.; Lin, X.; Hu, N.; Liao, J. Y.; Lin, L. B.; Zhao, C.; Hu, Z. M.; Liang, X.; Xu, W.; Chen, H.; Huang, W. BMP2 induces chondrogenic differentiation, osteogenic differentiation and endochondral ossification in stem cells. *Cell Tissue Res.* **2016**, *366* (1), 101–11.
- (40) Kwon, S. H.; Lee, T. J.; Park, J.; Hwang, J. E.; Jin, M.; Jang, H. K.; Hwang, N. S.; Kim, B. S. Modulation of BMP-2-induced chondrogenic versus osteogenic differentiation of human mesenchymal stem cells by cell-specific extracellular matrices. *Tissue Eng., Part A* **2013**, *19* (1–2), 49–58.
- (41) Maturavongsadit, P.; Luckanagul, J. A.; Metavarayuth, K.; Zhao, X.; Chen, L.; Lin, Y.; Wang, Q. Promotion of In Vitro Chondrogenesis of Mesenchymal Stem Cells Using In Situ Hyaluronic

Hydrogel Functionalized with Rod-Like Viral Nanoparticles. *Biomacromolecules* **2016**, *17* (6), 1930–1938.

- (42) Pacifici, M.; Golden, E. B.; Oshima, O.; Shapiro, I. M.; Leboy, P. S.; Adams, S. L. Hypertrophic chondrocytes. The terminal stage of differentiation in the chondrogenic cell lineage? *Ann. N. Y. Acad. Sci.* **1990**, 599, 45–57.
- (43) Pelttari, K.; Winter, A.; Steck, E.; Goetzke, K.; Hennig, T.; Ochs, B. G.; Aigner, T.; Richter, W. Premature induction of hypertrophy during in vitro chondrogenesis of human mesenchymal stem cells correlates with calcification and vascular invasion after ectopic transplantation in SCID mice. *Arthritis Rheum.* **2006**, *54* (10), 3254–66.
- (44) Yoo, J. U.; Johnstone, B. The role of osteochondral progenitor cells in fracture repair. *Clin. Orthop. Relat. Res.* **1998**, *355S*, *S73*–81.
- (45) Fuerst, M.; Bertrand, J.; Lammers, L.; Dreier, R.; Echtermeyer, F.; Nitschke, Y.; Rutsch, F.; Schäfer, F. K. W.; Niggemeyer, O.; Steinhagen, J.; Lohmann, C. H.; Pap, T.; Rüther, W. Calcification of articular cartilage in human osteoarthritis. *Arthritis Rheum.* **2009**, *60* (9), 2694–2703.
- (46) Mueller, M. B.; Tuan, R. S. Functional characterization of hypertrophy in chondrogenesis of human mesenchymal stem cells. *Arthritis Rheum.* **2008**, 58 (5), 1377–88.
- (47) Hall, A. Rho GTPases and the actin cytoskeleton. *Science* **1998**, 279 (5350), 509–14.
- (48) Teo, B. K.; Wong, S. T.; Lim, C. K.; Kung, T. Y.; Yap, C. H.; Ramagopal, Y.; Romer, L. H.; Yim, E. K. Nanotopography modulates mechanotransduction of stem cells and induces differentiation through focal adhesion kinase. *ACS Nano* **2013**, *7* (6), 4785–98.
- (49) Bhadriraju, K.; Yang, M.; Alom Ruiz, S.; Pirone, D.; Tan, J.; Chen, C. S. Activation of ROCK by RhoA is regulated by cell adhesion, shape, and cytoskeletal tension. *Exp. Cell Res.* **2007**, *313* (16), 3616–3623.